aerospace

MDPI

Article

Analysis of a Rigid-Body Pose Estimator for Relative Spacecraft Navigation

Caitong Peng [1] and Daniel Choukroun [2,*]

[1] Department of Electrical and Computer Engineering, Ben-Gurion University of the Negev, Beer-Sheva 84105, Israel; pengc@post.bgu.ac.il
[2] Department of Mechanical Engineering, Ben-Gurion University of the Negev, Beer-Sheva 84105, Israel
* Correspondence: danielch@bgu.ac.il

Abstract

This study presents a rigorous error analysis of a previously published estimator that determines the single-frame relative pose of two rigid bodies from batches of point and unit vector measurements. The estimator solves a constrained least-squares optimization problem where the pose is represented by a dual quaternion and the properties of pose dual quaternions are exactly satisfied. We develop an eigenvalue-based error analysis and derive analytical expressions for the three-dimensional attitude and translation errors, along with their means and covariance matrices. The closed-form formulas provide significant insights into the distinctive impacts of the point and vector observations' geometry and noise. They provide valuable tools for performance analysis and prediction. We consider noises both in the body frame and in the reference frame observations. Extensive Monte-Carlo simulations validate the accuracy and consistency of these formulas. Furthermore, we investigate the algorithm's sensitivity to variations in the number of observations and in the observations' weight coefficients of the cost function.

Keywords: pose estimation; dual quaternion; constrained estimation; stochastic error analysis; covariance analysis

1. Introduction

Accurate determination of the relative pose is fundamental for autonomous multiple-satellite flight missions. From proximity operations during rendezvous and docking to formation flying and orbital servicing, reliable pose estimates underpin critical onboard fault-tolerant guidance, navigation, and control (GNC) systems. Traditional relative pose representations in space GNC include quaternions augmented with relative orbital elements such as osculating elements or relative eccentricity/inclination vectors. These representations are valuable for time-varying filtering problems modeling the satellite's relative dynamics. Other representations are more adapted when considering the problem of single-frame relative pose estimation from images acquired by a putative vision system. Classical to computer vision are the essential matrix, the homogeneous transformation matrix, or a quaternion augmented with a position vector. However, these formulations either suffer from significant redundancy, yielding computational inefficiency, a lack of insight, or the arbitrary separation between rotational and translational components. In contrast, dual quaternions provide a compact and unified representation that elegantly encapsulates both rotation and translation within a single eight-parameter algebraic structure. Introduced in seminal works [1,2], they fully describe six degrees of freedom relative motions of rigid

Check for updates

Academic Editors: Gabriella Gaias and Jean-Sébastien Ardaens

Received: 1 November 2025
Revised: 11 December 2025
Accepted: 15 December 2025
Published: 26 December 2025

Copyright: © 2025 by the authors. Licensee MDPI, Basel, Switzerland. This article is an open access article distributed under the terms and conditions of the Creative Commons Attribution (CC BY) license.

bodies. The dual quaternion framework streamlines the mathematical treatment of spatial transformations, reducing both memory footprint and computational complexity compared with conventional matrix formulations. Over the past few decades, the dual quaternion has been successfully adopted for a range of aerospace applications. It has proven particularly effective in solving complex problems in spacecraft pose estimation [3,4], autonomous rendezvous and docking [5], and cooperative formation control [6].

This work is concerned with the problem of single-frame relative pose estimation from vector and point measurements, which are typical products of computer vision systems. Early methods optimize the rotation and the translation parameters separately [7,8], impairing the accuracy and the computation efficiency. A dual quaternion estimator was introduced in [9], which simultaneously determines orientation and position by minimizing a weighted cost function of the measurement errors. More recent pose estimators leverage deep learning approaches to effectively mitigate classical image processing shortcomings in spacecraft proximity operations [10]. A common drawback of early deterministic algorithms or recent powerful methods is the lack of stochastic error analysis.

With the purpose in mind of fusing single-frame pose estimates with other sensors' data within a broader time-varying filtering method, this work offers a stochastic error analysis of the dual quaternion estimator presented in [9]. The main contribution of this work is to provide a direct and computationally efficient way to quantify the estimator's uncertainty. We assume additive errors in both the body frame and the reference frame point and vector observations. The dual quaternion estimation errors are modeled as multiplicative errors both for the rotation quaternion and the dual part. This reduces the dimension analysis from eight to six, which is the minimal dimension for three-dimensional pose analysis. In the context of linear approximations, we derive closed-form expressions for the dual quaternion estimation error. The biases are shown to be zero under assumptions of unbiasedness and uncorrelation among the observations' noises. Closed-form expressions for the covariance matrices of the attitude and translation errors are developed as analytical functions of the observations and of the associated noise covariances. The statistical consistency of the proposed results is numerically demonstrated through comprehensive Monte-Carlo simulations within a large range of conditions. Finally, we further investigate the dual quaternion performances under various configurations of poses, point and vector batch sizes, noise levels, and weight coefficients in the cost function. The paper is organized as follows. Section 2 reviews the necessary mathematical background on dual quaternion algebra and presents the formulation and the solution of a batch pose estimation problem as a constrained least-squares optimization. Section 3 presents the systematic stochastic error analysis that yields novel and explicit analytical expressions for the attitude and translation error covariance matrices. Section 4 validates the analytical results via extensive MC simulations and evaluates the impact of the measurement noise level, the number of measurements, and the weighting parameters. Finally, Section 5 discusses the broader implications of the proposed framework for the design and analysis of autonomous aerospace systems and outlines promising directions towards real-time applications.

2. A Single-Frame Dual Quaternion Estimator

2.1. Dual Quaternion of the Rigid-Body Pose

The pose estimator studied in this work is a batch estimator of the dual quaternion from vector and point measurements. In this section, we briefly review the concept of dual quaternions and present the related estimator. Dual quaternions integrate dual numbers

and quaternions theories and enable a unified representation of rotations and translations in rigid-body kinematics. A dual quaternion, denoted by $\dot{q}$, is defined as

$$\dot{q} = \boldsymbol{q} + \epsilon \boldsymbol{q}_d, \tag{1}$$

where $\boldsymbol{q}$ and $\boldsymbol{q}_d$ are quaternions, denoting the real part and the dual part, respectively, of $\dot{q}$, and ϵ is a scalar that satisfies the idempotent property:

$$\epsilon^2 = 0 \tag{2}$$

A unit dual quaternion satisfies the following two constraints:

$$\boldsymbol{q}^T \boldsymbol{q} = 1 \tag{3}$$
$$\boldsymbol{q}_d{}^T \boldsymbol{q} = 0 \tag{4}$$

These constraints ensure that a dual quaternion unambiguously represents a rigid body transformation in three-dimensional space. The unity constraint in Equation (3) is the well-known unit-norm equation of rotation quaternions. Hence, the real part of $\dot{q}$ is a quaternion of rotation. The orthogonality constraint in Equation (4) further decreases the number of degrees of freedom to six, as should be for three-dimensional rigid body poses. The information on the translation component is encoded in the dual part, $\boldsymbol{q}_d$, and can be retrieved through well-known relationships, as will appear later. Compositions of rigid-body poses can be performed thanks to the multiplication of dual quaternions. Let $\dot{q}_1$ and $\dot{q}_2$ denote two dual quaternions with real and dual parts, $\boldsymbol{q}_1, \boldsymbol{q}_2, \boldsymbol{q}_{d1}, \boldsymbol{q}_{d2}$, respectively. The dual quaternion multiplication is defined as follows:

$$\dot{q}_1 \odot \dot{q}_2 = \begin{bmatrix} \boldsymbol{q}_1 \odot \boldsymbol{q}_2 \\ \boldsymbol{q}_{d1} \odot \boldsymbol{q}_2 + \boldsymbol{q}_1 \odot \boldsymbol{q}_{d2} \end{bmatrix} \tag{5}$$

where terms of the form $\boldsymbol{q}_1 \odot \boldsymbol{q}_2$ are quaternion multiplications, which is defined as follows:

$$\boldsymbol{q}_1 \odot \boldsymbol{q}_2 = \begin{bmatrix} \mathbf{e}_1 \times \mathbf{e}_2 + q_1 \mathbf{e}_2 + q_2 \mathbf{e}_1 \\ q_1 q_2 - \mathbf{e}_1^T \mathbf{e}_2 \end{bmatrix} \tag{6}$$

where $\mathbf{e}_1$, $\mathbf{e}_2, q_1, q_2$ denote the vector and scalar parts of $\boldsymbol{q}_1$ and $\boldsymbol{q}_2$, respectively. Notice that we have used the same symbol for quaternion and dual quaternion composition. This slight abuse of notation should not confuse, thanks to the context in which it is used. In the sequel, we will rely on the matrix representation of the multiplication operators, i.e., Equations (5) and (6) will be written as follows:

$$\dot{q}_1 \odot \dot{q}_2 = [\dot{q}_1 \odot] \dot{q}_2 \tag{7}$$

where

$$[\dot{q}_1 \odot] = \begin{bmatrix} [\boldsymbol{q}_1 \odot] & 0_{4\times4} \\ [\boldsymbol{q}_{d1} \odot] & [\boldsymbol{q}_1 \odot] \end{bmatrix} \tag{8}$$

and

$$[\boldsymbol{q} \odot] = \begin{bmatrix} [\,\mathbf{e} \times] + q I_3 & \mathbf{e} \\ -\,\mathbf{e}^T & q \end{bmatrix} \tag{9}$$

where I_3 denotes the identity matrix in $\mathbb{R}^3$.

2.2. Observation Model for the Dual Quaternion

Let $\mathcal{R}$ and $\mathcal{B}$ denote two right-hand Cartesian coordinate frames with different poses. Let us assume, without loss of generality, that $\mathcal{R}$ is a fixed frame and $\mathcal{B}$ is a moving frame and that we seek to estimate the pose of $\mathcal{B}$ with respect to $\mathcal{R}$. Let $D_{\mathcal{B}}^{\mathcal{R}}$ and $\mathrm{t}_{\mathcal{B}}^{\mathcal{R}}$ denote the traditional pose representation of $\mathcal{B}$ with respect to $\mathcal{R}$, i.e., the Directional Cosine Matrix, and the position vector from the origin of $\mathcal{B}$ to that of $\mathcal{R}$, expressed in $\mathcal{B}$. The pose estimator in [9] is a batch estimator of the dual quaternion that processes vector and point measurements. These measurements are modeled according to the frame-transformation relationships expressed using dual quaternions of the pose of $\mathcal{B}$ with respect to $\mathcal{R}$. It is valuable to first recall these relationships as a function of the DCM and position vector. Let $\mathrm{n_b}$ and $\mathrm{n_r}$ denote the projections of a physical unit vector on $\mathcal{B}$ and $\mathcal{R}$, respectively, then

$$\mathrm{n_b} = D\mathrm{n_r} \tag{10}$$

where D is to be interpreted as $D_{\mathcal{B}}^{\mathcal{R}}$. In vision-based pose estimation, the vector observation $(\mathrm{n_b}, \mathrm{n_r})$ may represent unit vectors associated with lines of sight, with edges, with control points segments, with surface normals, or, in general, associated with any extracted line. Assuming that a batch of such measurements is available, it is well known that three-dimensional rotation is observable if there are at least two simultaneous non-collinear vector observations. Let $\mathrm{p_b}$ and $\mathrm{p_r}$ denote the coordinates of a physical point in the $\mathcal{B}$ and $\mathcal{R}$ frames, respectively. Then the following geometrical relationship is satisfied:

$$\mathrm{p_b} = \mathrm{t} + D\mathrm{p_r} \tag{11}$$

where t denotes $\mathrm{t}_{\mathcal{B}}^{\mathcal{R}}$. Point observations, $\mathrm{p_b}, \mathrm{p_r}$, encapsulate information both on the translation and the rotation. Equations (10) and (11) summarize the ideal measurement model in terms of D and t. Typically, computer-vision systems extract batches of unit vectors and point measurements that are corrupted by errors and thus are not consistent. When the probabilistic models of these errors are unknown or difficult to analyze, one typically resorts to the universal method of least squares. The estimator in [9] is a least-squares estimator processing measurements of the type (10) and (11), expressed using dual quaternions. It can be shown that the frame-transformation Equations (10) and (11) can be written as follows:

$$\boldsymbol{n}_b = W(\boldsymbol{q})^T Q(\boldsymbol{q}) \boldsymbol{n}_r \tag{12}$$

$$\boldsymbol{p}_b = W(\boldsymbol{q})^T \boldsymbol{q}_d + W(\boldsymbol{q})^T Q(\boldsymbol{q}) \boldsymbol{p}_r \tag{13}$$

where $\boldsymbol{q}, \boldsymbol{q}_d$ are the real and dual parts of the dual quaternion, respectively, and all the other quantities are known parameters obtained from the point and vector observations. In particular, the parameters $\boldsymbol{n}$ and $\boldsymbol{p}$ are vectors and points expressed as 4×1 pure quaternions, i.e.,

$$\boldsymbol{n} = \begin{bmatrix} \mathrm{n} \\ 0 \end{bmatrix}, \boldsymbol{p} = \begin{bmatrix} \frac{1}{2}\mathrm{p} \\ 0 \end{bmatrix}, \tag{14}$$

in the body and reference frames. Hence, $\boldsymbol{p}_b, \boldsymbol{n}_b$ denote the point and vector observations in $\mathcal{B}$, and $\boldsymbol{p}_r, \boldsymbol{n}_r$ denote the point and vector observations in $\mathcal{R}$. The operators $Q(\boldsymbol{q})$ and $W(\boldsymbol{q})$ are 4×4 matrix functions of the rotation quaternion $\boldsymbol{q}$ corresponding to left- and right-quaternion multiplication, respectively. They are expressed as follows:

$$Q(\boldsymbol{q}) = \begin{bmatrix} [\mathbf{e}\times] + qI_3 & \mathbf{e} \\ -\mathbf{e}^T & q \end{bmatrix} \tag{15}$$

$$W(\boldsymbol{q}) = \begin{bmatrix} -[\mathbf{e}\times] + qI_3 & \mathbf{e} \\ -\mathbf{e}^T & q \end{bmatrix} \tag{16}$$

2.3. Pose Dual Quaternion Estimation [9]

Assuming that a batch of k vector observations and l point observations is available, a constrained least-squares problem is formulated as the following minimization problem:

$$\min_{\hat{\boldsymbol{q}},\hat{\boldsymbol{q}}_d} J = \sum_{i=1}^{k} \alpha_i \|\boldsymbol{n}_{b_i} - \hat{\boldsymbol{n}}_{b_i}\|^2 + \sum_{i=1}^{l} \beta_i \|\boldsymbol{p}_{b_i} - \hat{\boldsymbol{p}}_{b_i}\|^2 \tag{17}$$

subject to the unit dual quaternion constraints:

$$\hat{\boldsymbol{q}}^T \hat{\boldsymbol{q}} = 1 \tag{18}$$

$$\hat{\boldsymbol{q}}^T \hat{\boldsymbol{q}}_d = 0 \tag{19}$$

The quantities $\boldsymbol{n}_{b_i}$ and $\boldsymbol{p}_{b_i}$ are the noisy point and vector measurements, while the quantities $\hat{\boldsymbol{n}}_{b_i}$ and $\hat{\boldsymbol{p}}_{b_i}$ are their predictions calculated by inserting $\hat{\boldsymbol{q}}, \hat{\boldsymbol{q}}_d$ in the right-hand sides of (12) and (13). The weights α_i and β_i are positive coefficients that are assigned according to the relative reliability of the i point and vector measurement. These reliabilities are typically reciprocal functions of the variances of the random errors associated with the measurements, which depend on errors in the body observations and in the reference observations. The above minimization problem is nonlinear in the dual quaternion components because of the nonlinear nature of the observation model equations and of the constraints. The solution is summarized in the following algorithm.

Pose Estimator Summary:

Let C_1, C_2, and C_3 denote the following 4×4 matrices:

$$C_1 = -2 \sum_{i=1}^{k} \alpha_i Q(\boldsymbol{n}_{b_i})^T W(\boldsymbol{n}_{r_i}) - 2 \sum_{i=1}^{l} \beta_i Q(\boldsymbol{p}_{b_i})^T W(\boldsymbol{p}_{r_i}) \tag{20}$$

$$C_2 = \beta\, I_4 \tag{21}$$

$$C_3 = 2 \sum_{i=1}^{l} \beta_i \left[W(\boldsymbol{p}_{r_i}) - Q(\boldsymbol{p}_{b_i}) \right] \tag{22}$$

where $\beta = \sum_{i=1}^{l} \beta_i$, and let the 4×4 matrix A be constructed as follows:

$$A = \frac{1}{2} [C_3^T (C_2 + C_2^T)^{-1} C_3 - (C_1 + C_1^T)] \tag{23}$$

The optimal rotation quaternion estimate $\boldsymbol{q}$ that solves problem (17) under conditions (18) and (19) is the eigenvector of A from (23) associated with the maximal eigenvalue:

$$A\boldsymbol{q} = \lambda_{max} \boldsymbol{q} \tag{24}$$

Furthermore, the optimal estimate of the dual part $\boldsymbol{q_d}$ is calculated by solving a linear system of equations as follows:

$$\boldsymbol{q_d} = -(C_2 + C_2^T)^{-1} C_3^T \boldsymbol{q} \tag{25}$$

The algorithm, Equations (20)–(25), solves a global nonlinear pose estimation problem without resorting to linearization. It invokes an eigenvalue/eigenvector solver for the rotation part. The computation burden is dominated by the rotation solution since the translation solution only adds linear equations. In the particular case where only unit vector measurements are available, the above optimization problem and its solution boil down to the well-known q-method, see Section 5.3.1 in [11], i.e., Davenport's quaternion solution of the famous Wahba problem. This estimator belongs to the family of methods building motion from structure: it assumes enough prior information on the observed object to build the reference point and vector observations. If the position vector is ultimately the parameter of interest, it is straightforward to obtain it via the following identity:

$$\begin{bmatrix} \mathrm{t} \\ 0 \end{bmatrix} = 2W(\boldsymbol{q})^T \boldsymbol{q_d} \tag{26}$$

3. Estimation Error Analysis

This section presents a detailed error analysis of the dual quaternion estimator described previously. We consider an 8×1 dual quaternion multiplicative error first by exploiting the physical insight of motion composition using dual quaternions. Then we derive expressions for the 3×1 rotation error vector $\boldsymbol{\delta\theta}$ and the 3×1 translation error vector $\mathbf{\Delta t}$. Finally, linear approximations are developed for the first two moments of the estimation errors, under typical assumptions on the point and vector observation errors. These expressions are of great value since they quantify the uncertainty present in the dual quaternion estimate. Their validity and statistical consistency are tested in the subsequent section.

3.1. Dual Quaternion Multiplicative Error

By analogy with quaternion estimation, we adopt a multiplicative error approach to model the estimation error. Let $\mathcal{R}$, $\mathcal{B}$, and $\hat{\mathcal{B}}$ denote the reference frame, the true body frame, and the estimated body frame, respectively. Then the dual quaternion composition described earlier naturally lends itself to a geometrical definition of the pose estimation error as the dual quaternion representing the pose of $\hat{\mathcal{B}}$ with respect to $\mathcal{B}$. It is defined by the following equation, which describes the successive rigid-body motion from $\mathcal{R}$ to $\mathcal{B}$, and from $\mathcal{B}$ to $\hat{\mathcal{B}}$:

$$q_{\hat{\mathcal{B}}}^{\mathcal{R}} = q_{\mathcal{B}}^{\mathcal{R}} \odot q_{\hat{\mathcal{B}}}^{\mathcal{B}} \tag{27}$$

Rewriting Equation (27) in the simplified notation of Equation (28) emphasizes that δq represents a multiplicative rather than an additive dual quaternion error. Thanks to this multiplicative representation, the unit-norm and orthogonality constraint inherent to dual quaternions are preserved. It ensures that the error δq has a clear geometric interpretation as a pose transformation.

$$\hat{q} = q^t \odot \delta q \tag{28}$$

where superscript t denotes the true value of the underlying variable. Expanding Equation (28) yields Equation (29), which decomposes the pose error into its rotational component $\delta \boldsymbol{q}$ and its coupled rotation and translation component $\delta \boldsymbol{q_d}$.

$$\begin{aligned} \hat{q} &= (\boldsymbol{q}^t + \epsilon \boldsymbol{q_d}^t) \odot (\delta \boldsymbol{q} + \epsilon \delta \boldsymbol{q_d}) \\ &= (\boldsymbol{q}^t \odot \delta \boldsymbol{q}) + \epsilon (\boldsymbol{q_d}^t \odot \delta \boldsymbol{q} + \boldsymbol{q}^t \odot \delta \boldsymbol{q_d}) \end{aligned} \tag{29}$$

where the second line stems from applying the property $\epsilon^2 = 0$. We proceed with the parametrization of the 4×1 error vector $\delta \boldsymbol{q}$ via an 3×1 Euler vector $\boldsymbol{\delta\theta}$. Consider a small rotation error characterized by an axis-angle representation, with rotation angle $\theta = \|\boldsymbol{\delta\theta}\|$ and unit axis $\mathbf{u} = \boldsymbol{\delta\theta}/\|\boldsymbol{\delta\theta}\|$. The exact error quaternion is expressed as follows:

$$\begin{aligned} \delta \boldsymbol{q} &= \begin{bmatrix} \mathbf{u} \sin(\theta/2) \\ \cos(\theta/2) \end{bmatrix} \\ &= \begin{bmatrix} \frac{\boldsymbol{\delta\theta}}{\|\boldsymbol{\delta\theta}\|} \sin(\|\boldsymbol{\delta\theta}\|/2) \\ \cos(\|\boldsymbol{\delta\theta}\|/2) \end{bmatrix} \end{aligned} \tag{30}$$

Applying Taylor series expansions around $\|\boldsymbol{\delta\theta}\| = 0$ yields:

$$\begin{aligned} \sin(\|\boldsymbol{\delta\theta}\|/2) &= \frac{\|\boldsymbol{\delta\theta}\|}{2} - \frac{\|\boldsymbol{\delta\theta}\|^3}{48} + \mathcal{O}(\|\boldsymbol{\delta\theta}\|^5) \\ &\approx \frac{\|\boldsymbol{\delta\theta}\|}{2} \end{aligned} \tag{31}$$

$$\begin{aligned} \cos(\|\boldsymbol{\delta\theta}\|/2) &= 1 - \frac{\|\boldsymbol{\delta\theta}\|^2}{8} + \mathcal{O}(\|\boldsymbol{\delta\theta}\|^4) \\ &\approx 1 \end{aligned} \tag{32}$$

Substituting Equations (31) and (32) into Equation (30) and keeping the first-order terms yields the widely applied approximation:

$$\delta \boldsymbol{q} \simeq \begin{bmatrix} \frac{1}{2}\boldsymbol{\delta\theta} \\ 1 \end{bmatrix} \tag{33}$$

We apply a similar approach to obtain a minimal parametrization of the 4×1 error vector $\delta \boldsymbol{q_d}$ using a 3×1 translation error $\mathbf{\Delta t}$. Inserting the multiplicative quaternion error and the translation error in (26) yields:

$$\delta \boldsymbol{q_d} = \frac{1}{2} W(\delta \boldsymbol{q}) \begin{bmatrix} \mathbf{\Delta t} \\ 0 \end{bmatrix} \tag{34}$$

Expanding the quaternion multiplication and neglecting the second-order coupling terms yields:

$$\begin{aligned} \delta \boldsymbol{q_d} &= \frac{1}{2} \begin{bmatrix} \mathbf{\Delta t} - [\frac{1}{2}\boldsymbol{\delta\theta}]_\times \mathbf{\Delta t} \\ -\frac{1}{2}\boldsymbol{\delta\theta}^T \mathbf{\Delta t} \end{bmatrix} \\ &\simeq \begin{bmatrix} \frac{1}{2}\mathbf{\Delta t} \\ 0 \end{bmatrix} \end{aligned} \tag{35}$$

Substituting (33) and (35) in (29) yields the following expression for the estimated dual quaternion:

$$\hat{\mathcal{q}} = \left(\boldsymbol{q}^t \odot \begin{bmatrix} \frac{1}{2}\boldsymbol{\delta\theta} \\ 1 \end{bmatrix} \right) + \epsilon \left(\boldsymbol{q_d}^t \odot \begin{bmatrix} \frac{1}{2}\boldsymbol{\delta\theta} \\ 1 \end{bmatrix} + \boldsymbol{q}^t \odot \begin{bmatrix} \frac{1}{2}\boldsymbol{\Delta t} \\ 0 \end{bmatrix} \right) \tag{36}$$

Equation (36) can be further simplified by applying the concept of sequential pose transformation, which is explained next. The proposed estimator provides a dual quaternion of the pose from frame $\mathcal{R}$ to frame $\hat{\mathcal{B}}$, $\mathcal{q}_{\hat{\mathcal{B}}}^{\mathcal{R}}$. Suppose that there is another reference frame $\mathcal{R}'$ in which we prefer processing the observations, and that the relative pose of $\mathcal{R}'$ with respect to $\mathcal{R}$ is known. Let the latter be denoted by $\mathcal{q}_{\mathcal{R}'}^{\mathcal{R}}$. Then, the same estimator can be used to estimate the pose $\mathcal{q}_{\hat{\mathcal{B}}}^{\mathcal{R}'}$. Although the pose estimates differ, it is obvious that the estimation error, $\mathcal{q}_{\hat{\mathcal{B}}}^{\mathcal{B}}$, is identical in both cases. Since the choice of $\mathcal{R}'$ is arbitrary, one can choose the body frame $\mathcal{B}$. This choice yields simple expressions for the true dual quaternion $\mathcal{q}^t$ in (36), i.e.,

$$\boldsymbol{q}^t = \begin{bmatrix} 0_3 \\ 1 \end{bmatrix} \tag{37}$$

$$\boldsymbol{q_d}^t = \begin{bmatrix} 0_3 \\ 0 \end{bmatrix} \tag{38}$$

where $0_3 \in \mathbb{R}^3$ denotes the 3×1 zero vector. Using (37) and (38) in (36) yields the simplified expression that will be used in the sequel.

3.2. Linear Error Analysis

Let $\mathrm{n_{b_i}}$, $\mathrm{p_{b_i}}$ denote the body vector and point observations, respectively, and let $\mathrm{n_{r_i}}$ and $\mathrm{p_{r_i}}$ denote the reference vector and point observations, respectively. In this study, we assume that all observations are corrupted by errors. At this point, these errors may encompass biases, white noise, and any necessary error, deterministic or stochastic. Typical assumptions carried in error analysis often focus on body measurement errors, neglecting reference-related errors. The reference observations are, however, often derived from prior image processing, e.g., image registration, mapping, and scene reconstruction, and are thus themselves entailed with errors worth considering. The coefficients α_i and β_i are therefore to be interpreted as a combined reliability of the body and reference observations. For the sake of simplicity, the errors are assumed to be additive, as follows:

$$\mathrm{n_{b_i}} = \mathrm{n_{b_i}^t} + \Delta\mathrm{n_{b_i}} \tag{39}$$

$$\mathrm{n_{r_i}} = \mathrm{n_{b_i}^t} + \Delta\mathrm{n_{r_i}} \tag{40}$$

$$\mathrm{p_{b_i}} = \mathrm{p_{b_i}^t} + \Delta\mathrm{p_{b_i}} \tag{41}$$

$$\mathrm{p_{r_i}} = \mathrm{p_{b_i}^t} + \Delta\mathrm{p_{r_i}} \tag{42}$$

Notice that the true observations are identical in the reference and body frames but that the errors might differ since their causes are different. The objective of this error analysis is to study the perturbed eigenvector/eigenvalue Equation (24) that underlines the optimal quaternion estimator. It is rewritten here for convenience:

$$A\hat{\boldsymbol{q}} = \lambda_{max}\hat{\boldsymbol{q}} \tag{43}$$

where A and λ_{max} are calculated from the noisy information $\mathrm{n_{b_i}}$, $\mathrm{p_{b_i}}$, $\mathrm{n_{r_i}}$ and $\mathrm{p_{r_i}}$. Equation (43) is rewritten next using perturbation quantities, as follows:

$$(A_0 + \Delta A)(\boldsymbol{q}^t \odot \delta\boldsymbol{q}) = (\lambda_0 + \Delta\lambda)(\boldsymbol{q}^t \odot \delta\boldsymbol{q}) \tag{44}$$

where A_0 is constructed using the true observations, λ_0 is its maximum eigenvalue, and ΔA and $\Delta\lambda$ are the associated perturbations due to the observations errors. Using (33) and (37) in (44) yields:

$$(A_0 + \Delta A)\left(\begin{bmatrix}0_3\\1\end{bmatrix} + \frac{1}{2}\begin{bmatrix}\boldsymbol{\delta\theta}\\0\end{bmatrix}\right) = (\lambda_0 + \Delta\lambda)\left(\begin{bmatrix}\mathbf{0_3}\\1\end{bmatrix} + \frac{1}{2}\begin{bmatrix}\boldsymbol{\delta\theta}\\0\end{bmatrix}\right) \tag{45}$$

Expanding (45), the zeroth-order terms on both sides cancel each other, and the second-order terms are neglected, which yields the following identity involving first-order terms with respect to the perturbations ΔA, $\boldsymbol{\delta\theta}$, and $\Delta\lambda$:

$$\frac{1}{2}A_0\begin{bmatrix}\boldsymbol{\delta\theta}\\0\end{bmatrix} + \Delta A\begin{bmatrix}0_3\\1\end{bmatrix} = \frac{1}{2}\lambda_0\begin{bmatrix}\boldsymbol{\delta\theta}\\0\end{bmatrix} + \Delta\lambda\begin{bmatrix}0_3\\1\end{bmatrix} \tag{46}$$

Let the 4×4 matrices A_0 and ΔA be partitionned as follows:

$$A_0 = \begin{bmatrix}A_0(1,1) & A_0(1,2)\\A_0(2,1) & A_0(2,2)\end{bmatrix} \tag{47}$$

$$\Delta A = \begin{bmatrix}\Delta A(1,1) & \Delta A(1,2)\\\Delta A(2,1) & \Delta A(2,2)\end{bmatrix} \tag{48}$$

such that $A_0(1,1)$ and $\Delta A(1,1)$ are 3×3 submatrices, and the dimensions of the other submatrices are defined accordingly. Substituting (47) and (48) into (46) yields the following expressions for the error vector $\boldsymbol{\delta\theta}$ and the eigenvalue perturbation $\Delta\lambda$:

$$\boldsymbol{\delta\theta} = 2[\lambda_0 I_3 - A_0(1,1)]^{-1}\,\Delta A(1,2) \tag{49}$$

$$\Delta\lambda = A_0(2,1)\,[\lambda_0 I_3 - A_0(1,1)]^{-1}\,\Delta A(1,2) \;+\; \Delta A(2,2) \tag{50}$$

While the important result is the expression for $\boldsymbol{\delta\theta}$, it is still valuable to obtain the perturbation $\Delta\lambda$ as a function of the observations and their errors. It will now be shown that the latter is zero to first order, and that more insight into the former can be obtained. The partition of the matrix A_0 is derived from (20)–(23), as follows:

$$A_0 = 2\begin{bmatrix}B_{0n} + B_{0p} - 2B_0 & 0_3\\ {0_3}^T & \sum_{i=1}^{k}\alpha_i + \sum_{i=1}^{l}\beta_i {\mathrm{p}_{\mathrm{b_i}}^t}^T \mathrm{p}_{\mathrm{b_i}}^t\end{bmatrix} \tag{51}$$

where

$$B_{0n} = \sum_{i=1}^{k}\alpha_i\left([\mathrm{n}_{\mathrm{b_i}}^t\times][\mathrm{n}_{\mathrm{b_i}}^t\times] + \mathrm{n}_{\mathrm{b_i}}^t {\mathrm{n}_{\mathrm{b_i}}^t}^T\right) \tag{52}$$

$$B_{0p} = \sum_{i=1}^{l}\beta_i\left([\mathrm{p}_{\mathrm{b_i}}^t\times][\mathrm{p}_{\mathrm{b_i}}^t\times] + \mathrm{p}_{\mathrm{b_i}}^t {\mathrm{p}_{\mathrm{b_i}}^t}^T\right) \tag{53}$$

$$B_0 = \frac{1}{\beta}\sum_{i,j=1}^{l}\beta_i\beta_j\left([\mathrm{p}_{\mathrm{b_i}}^t\times][\mathrm{p}_{\mathrm{b_j}}^t\times]\right) \tag{54}$$

where

$$\beta = \sum_{i=1}^{l} \beta_i \tag{55}$$

The important results here are that

$$A_0(1,1) = 2(B_{0n} + B_{0p} - 2B_0) \tag{56}$$

$$A_0(2,1) = 0_3 \tag{57}$$

The first-order perturbation on the matrix ΔA is derived using (23) via first-order perturbations on C_1, C_2, and C_3:

$$\Delta A = \frac{1}{2}(-\Delta C_1 - \Delta C_1^T + \Delta C_3 C_2^{-1} C_3^T + C_3 C_2^{-1} \Delta C_3^T) \tag{58}$$

where we used the property that C_2 is a scaled identity matrix. The expressions for $\Delta C_1, \Delta C_3$ are defined as follows:

$$\Delta C_1 = -2 \sum_{i=1}^{k} \alpha_i [Q(\boldsymbol{n}_{b_i})^T W(\Delta \boldsymbol{n}_{r_i}) + Q(\Delta \boldsymbol{n}_{b_i})^T W(\boldsymbol{n}_{r_i})] \tag{59}$$

$$-2 \sum_{i=1}^{l} \beta_i [Q(\boldsymbol{p}_{b_i})^T W(\Delta \boldsymbol{p}_{r_i}) + Q(\Delta \boldsymbol{p}_{b_i})^T W(\boldsymbol{p}_{r_i})] \tag{60}$$

$$\Delta C_3 = 2 \sum_{i=1}^{l} \beta_i \left[W(\Delta \boldsymbol{p}_{r_i}) - Q(\Delta \boldsymbol{p}_{b_i}) \right] \tag{61}$$

Then, the derivation of ΔA is lengthy but straightforward, which yields the following expression:

$$\Delta A = \begin{bmatrix} (\Delta B_n + \Delta B_p - 2\Delta B) + (\Delta B_n + \Delta B_p - 2\Delta B)^T & 2(\Delta Z_n + \Delta Z_p + \Delta Z) \\ 2(\Delta Z_n + \Delta Z_p + \Delta Z)^T & 0 \end{bmatrix} \tag{62}$$

where

$$\Delta B_n = \sum_{i=1}^{k} \alpha_i \left[\mathrm{n}_{\mathrm{b_i}}^t \times]([\Delta \mathrm{n}_{\mathrm{b_i}} \times] - [\Delta \mathrm{n}_{\mathrm{r_i}} \times]) + \Delta \mathrm{n}_{\mathrm{r_i}} \mathrm{n}_{\mathrm{b_i}}^{t\ T} + \mathrm{n}_{\mathrm{b_i}}^t \Delta \mathrm{n}_{\mathrm{b_i}}^{\ T} \right] \tag{63}$$

$$\Delta B_p = \sum_{i=1}^{l} \beta_i \left[[\mathrm{p}_{\mathrm{b_i}}^t \times]([\Delta \mathrm{p}_{\mathrm{b_i}} \times] - [\Delta \mathrm{p}_{\mathrm{r_i}} \times]) + \Delta \mathrm{p}_{\mathrm{r_i}} \mathrm{p}_{\mathrm{b_i}}^{t\ T} + \mathrm{p}_{\mathrm{b_i}}^t \Delta \mathrm{p}_{\mathrm{b_i}}^{\ T} \right] \tag{64}$$

$$\Delta B = \frac{1}{\beta} \sum_{i,j=1}^{l} \beta_i \beta_j \left[[\mathrm{p}_{\mathrm{b_i}}^t \times]([\Delta \mathrm{p}_{\mathrm{r_j}} \times] + [\Delta \mathrm{p}_{\mathrm{b_j}} \times]) \right] \tag{65}$$

$$\Delta Z_n = \sum_{i=1}^{k} \alpha_i \left[[\mathrm{n}_{\mathrm{b_i}}^t \times](\Delta \mathrm{n}_{\mathrm{b_i}} - \Delta \mathrm{n}_{\mathrm{r_i}}) \right] \tag{66}$$

$$\Delta Z_p = \sum_{i=1}^{l} \beta_i \left[[\mathrm{p}_{\mathrm{b_i}}^t \times](\Delta \mathrm{p}_{\mathrm{b_i}} - \Delta \mathrm{p}_{\mathrm{r_i}}) \right] \tag{67}$$

$$\Delta Z = \frac{1}{\beta} \sum_{i,j=1}^{l} \beta_i \beta_j \left[[\mathrm{p}_{\mathrm{b_i}}^t \times](\Delta \mathrm{p}_{\mathrm{r_j}} - \Delta \mathrm{p}_{\mathrm{b_j}}) \right] \tag{68}$$

The important results about ΔA are that

$$\Delta A(1,2) = 2(\Delta Z_n + \Delta Z_p + \Delta Z) \tag{69}$$

$$\Delta A(2,2) = 0 \tag{70}$$

Finally, using (56), (57), (69) and (70) in (71), (72) yields the sought expressions for $\boldsymbol{\delta\theta}$, and the confirmation that $\Delta\lambda$ is zero to first-order in the observation errors:

$$\boldsymbol{\delta\theta} = 2\left[\frac{1}{2}\lambda_0 I_3 - (B_{0n} + B_{0p} - 2B_0)\right]^{-1}(\Delta Z_n + \Delta Z_p + \Delta Z) \tag{71}$$

$$\Delta\lambda = 0 \tag{72}$$

Turning to the analysis of the translational error, we start with the estimation equation, which is rewritten next:

$$\hat{\boldsymbol{q}}_d = -(2C_2)^{-1}C_3^T\hat{\boldsymbol{q}} \tag{73}$$

Using the dual component in the right-hand side (RHS) of (36) to express the left-hand side of (73), and expanding the terms in the RHS of (73) with first-order perturbations yields the following relationship:

$$\left(\boldsymbol{q}_d{}^t \odot \begin{bmatrix}\frac{1}{2}\boldsymbol{\delta\theta}\\ 1\end{bmatrix} + \boldsymbol{q}^t \odot \begin{bmatrix}\frac{1}{2}\mathbf{\Delta t}\\ 0\end{bmatrix}\right) = -(2C_2)^{-1}(C_3^0 + \Delta C_3)^T\left(\boldsymbol{q}^t \odot \begin{bmatrix}\frac{1}{2}\boldsymbol{\delta\theta}\\ 1\end{bmatrix}\right) \tag{74}$$

Inserting (37) and (38) in (74) yields:

$$\begin{bmatrix}\frac{1}{2}\mathbf{\Delta t}\\ 0\end{bmatrix} = -(2C_2)^{-1}(C_3^0 + \Delta C_3)^T\begin{bmatrix}\frac{1}{2}\boldsymbol{\delta\theta}\\ 1\end{bmatrix} \tag{75}$$

Using the definitions of C_2 and C_3 in (75) finally yields the expression of the translational error $\mathbf{\Delta t}$.

Summary of the Linear Error Analysis

The linear errors in rotation and translation associated with the estimator under study are summarized next:

$$\boldsymbol{\delta\theta} = 2\left[\frac{1}{2}\lambda_0 I_3 - (B_{0n} + B_{0p} - 2B_0)\right]^{-1}(\Delta Z_n + \Delta Z_p + \Delta Z) \tag{76}$$

$$\mathbf{\Delta t} = \frac{2}{\beta}\left[\left(\sum_{i=1}^{l}\beta_i[\mathrm{p}_{\mathrm{b_i}}^t\times]\right)\boldsymbol{\delta\theta} - \sum_{i=1}^{l}\beta_i(\Delta\mathrm{p}_{\mathrm{r_i}} - \Delta\mathrm{p}_{\mathrm{b_i}})\right] \tag{77}$$

where

$$\beta = \sum_{i=1}^{l}\beta_i \tag{78}$$

$$B_{0n} = \sum_{i=1}^{k}\alpha_i\left([\mathrm{n}_{\mathrm{b_i}}^t\times][\mathrm{n}_{\mathrm{b_i}}^t\times] + \mathrm{n}_{\mathrm{b_i}}^t\mathrm{n}_{\mathrm{b_i}}^{t\ T}\right) \tag{79}$$

$$B_{0p} = \sum_{i=1}^{l}\beta_i\left([\mathrm{p}_{\mathrm{b_i}}^t\times][\mathrm{p}_{\mathrm{b_i}}^t\times] + \mathrm{p}_{\mathrm{b_i}}^t\mathrm{p}_{\mathrm{b_i}}^{t\ T}\right) \tag{80}$$

$$B_0 = \frac{1}{\beta}\sum_{i,j=1}^{l}\beta_i\beta_j\left([\mathrm{p}_{\mathrm{b_i}}^t\times][\mathrm{p}_{\mathrm{b_j}}^t\times]\right) \tag{81}$$

and

$$\Delta Z_n = \sum_{i=1}^{k} \alpha_i \left[[\mathrm{n}_{\mathrm{b_i}}^t \times] (\Delta \mathrm{n}_{\mathrm{b_i}} - \Delta \mathrm{n}_{\mathrm{r_i}}) \right] \tag{82}$$

$$\Delta Z_p = \sum_{i=1}^{l} \beta_i \left[[\mathrm{p}_{\mathrm{b_i}}^t \times] (\Delta \mathrm{p}_{\mathrm{b_i}} - \Delta \mathrm{p}_{\mathrm{r_i}}) \right] \tag{83}$$

$$\Delta Z = \frac{1}{\beta} \sum_{i,j=1}^{l} \beta_i \beta_j \left[[\mathrm{p}_{\mathrm{b_i}}^t \times] (\Delta \mathrm{p}_{\mathrm{r_j}} - \Delta \mathrm{p}_{\mathrm{b_j}}) \right] \tag{84}$$

The main result of this section is that the errors in rotation and translation are amenable to explicit linear mappings of the errors in the body and reference vector and point observations. These mappings are deterministic since they are functions of the true values of the observations. This assumption forms the backbone for the derivations of the first two probabilistic moments of the pose estimation errors, which are presented in the next section. The expressions in (76)–(84) provide an explicit link between the measurement noise in the body and reference frames and the resulting errors in the estimated dual quaternion. In particular, the perturbation terms ΔZ_n, ΔZ_p, and ΔZ represent three distinct pathways through which the observation noise corrupts the pose estimate. The term ΔZ_n describes the effect of noise in the vector observations. The cross-product operation in Equation (82) transforms the difference between body and reference vector observation errors into a rotational perturbation. Physically, this operation captures the fact that any deviation in the observed vector from its true direction corresponds to an angular error. Since vectors are of unit length, these errors translate to angular deviations without scaling effects. The cross-product structure implies that errors perpendicular to $\mathrm{n}_{\mathrm{b_i}}^t$ contribute maximally to the rotation estimation error, while errors parallel to $\mathrm{n}_{\mathrm{b_i}}^t$ vanish. Moreover, the geometric amplification is determined by the angle between the error direction and the vector direction. The summation over all k observations with weights α_i aggregates these contributions, with higher weights emphasizing more reliable vector observations. The magnitude of the term ΔZ_p is proportional to the distance of the point from the frame origin. Consequently, points located farther from the origin amplify the impact of the position noise. The term ΔZ captures the interaction among all point measurements. It is induced by the batch formulation that introduces cross-coupling between the geometry of one point and the noise of another. This effect is unique to joint pose estimation using point features and has no counterpart in purely vector-based attitude estimation problems such as Wahba's formulation. These perturbations are premultiplied by matrices constructed from the true geometric configuration of the observed features, namely B_{0n}, B_{0p}, and B_0. These matrices encode the spatial distribution and orientation of the observed vectors and points, and therefore act as sensitivity matrices that depend on the geometry of the scene. Consequently, the same level of measurement noise can induce significantly different pose errors under different feature configurations. In particular, geometries that lead to a badly conditioned matrix $(B_{0n} + B_{0p} - 2B_0)$ will amplify noise and increase the magnitude of $\boldsymbol{\delta\theta}$ and $\mathbf{\Delta t}$, whereas a good geometry will naturally attenuate their effect. These relationships make clear that the dual quaternion pose error is not solely a function of the observation noise magnitude, but rather of the combined interaction between noise statistics and the underlying spatial geometry of the features.

3.3. Estimation Error Covariance Analysis

3.3.1. Stochastic Model Assumptions on the Observation Errors

The errors in the body observations depend on the sensors and their internal parameters, while the errors in the reference observations usually depend on models. For

instance, point and vector body observations from an image depend on the pixel point spread function, pixel quantization, uncertainty on the focal distance, pixel dimensions, and image central point. On the other hand, point and vector reference observations from an image depend on the accuracy of the mapping of the object under observation. They also depend on the accuracy of the association between body and reference points, which is achieved through image registration. For the sake of generality, we will assume in this study that all errors are unbiased. While reference errors may be assumed as such, body errors are unlikely to be free of biases. Nevertheless, this assumption is pertinent on the account that sensors are usually calibrated before integration on the ground, and that these calibration tests take care of most of the deterministic errors, i.e., the biases. We will thus assume that the expectations of all basic errors are zero, as follows:

$$E\{\Delta \mathrm{n}_{r_i}\} = E\{\Delta \mathrm{n}_{\mathrm{b}_i}\} = E\{\Delta \mathrm{p}_{\mathrm{r}_i}\} = E\{\Delta \mathrm{p}_{\mathrm{b}_i}\} = \mathbf{0_3} \tag{85}$$

where $i = 1, \ldots, k$ for the vector observations, and $i = 1, \ldots, l$ for the point observations. Let $R_{\mathrm{n}_{\mathrm{b}_i}}, R_{\mathrm{n}_{\mathrm{r}_i}}, R_{\mathrm{p}_{\mathrm{b}_i}}, R_{\mathrm{p}_{\mathrm{r}_i}}$ denote the covariance matrices of additive errors in the vector and point observations, as observed in the body and reference frames, respectively. Applying assumptions (85) yields the following identities:

$$R_{\mathrm{n}_{\mathrm{b}_i}} = E\{\Delta \mathrm{n}_{\mathrm{b}_i} \Delta \mathrm{n}_{\mathrm{b}_i}{}^T\} \tag{86}$$

$$R_{\mathrm{n}_{\mathrm{r}_i}} = E\{\Delta \mathrm{n}_{\mathrm{r}_i} \Delta \mathrm{n}_{\mathrm{r}_i}{}^T\} \tag{87}$$

$$R_{\mathrm{p}_{\mathrm{b}_i}} = E\{\Delta \mathrm{p}_{\mathrm{b}_i} \Delta \mathrm{p}_{\mathrm{b}_i}{}^T\} \tag{88}$$

$$R_{\mathrm{p}_{\mathrm{r}_i}} = E\{\Delta \mathrm{p}_{\mathrm{r}_i} \Delta \mathrm{p}_{\mathrm{r}_i}{}^T\} \tag{89}$$

where $i = 1, \ldots, k$ for the vector observations, and $i = 1, \ldots, l$ for the point observations. Furthermore, we assume that the body and reference vector observations are mutually uncorrelated. This is the case, for instance, when the observations are acquired by different spacecraft sensors, e.g., a sun sensor, a magnetometer, a star tracker. However, this assumption still holds if we assume that all vector observations are acquired via processing a single-frame image from a star-tracker, provided that the deterministic joint errors have been compensated. Similarly, we assume that the body point observations are mutually uncorrelated, and that the reference point observations are mutually uncorrelated, too. This is pertinent if we assume that all point observations are acquired via a single-frame image from a camera, provided that the deterministic joint errors have been compensated. Henceforth, the following identities hold:

$$E\{\Delta \mathrm{n}_{\mathrm{b}_i} \Delta \mathrm{n}_{\mathrm{b}_j}{}^T\} = E\{\Delta \mathrm{n}_{\mathrm{r}_i} \Delta \mathrm{n}_{\mathrm{r}_j}{}^T\} = E\{\Delta \mathrm{p}_{\mathrm{b}_i} \Delta \mathrm{p}_{\mathrm{b}_j}{}^T\} = E\{\Delta \mathrm{p}_{\mathrm{r}_i} \Delta \mathrm{p}_{\mathrm{r}_j}{}^T\} = 0, \quad i \neq j \tag{90}$$

In addition, it is assumed that there is no cross-correlation between the errors in the body and the reference observations. This assumption is applied to both point and vector measurements. It makes sense when the error sources are independent: body observations are corrupted by on-board sensor electronics, while reference observations depend on tables or models. Similarly, zero cross-correlations are assumed between errors in body vectors and reference points, and vice versa. Notice that body vectors and body points error cross-correlation are not necessarily zero in this study. Indeed, if vectors are constructed using point pairs, such cross-correlations may exist. This study assumes that all point and vector observations are independently acquired. To sum-up, the lack of cross-correlations among the point and vector observations is expressed as follows:

$$E\{\Delta \mathrm{n}_{\mathrm{b}_i} \Delta \mathrm{n}_{\mathrm{r}_i}{}^T\} = E\{\Delta \mathrm{p}_{\mathrm{b}_i} \Delta \mathrm{p}_{\mathrm{r}_i}{}^T\} = E\{\Delta \mathrm{n}_{\mathrm{b}_i} \Delta \mathrm{p}_{\mathrm{r}_i}{}^T\} = E\{\Delta \mathrm{n}_{\mathrm{r}_i} \Delta \mathrm{p}_{\mathrm{b}_i}{}^T\} = 0 \tag{91}$$

where $i = 1, \ldots, k$ for the vector observations, and $i = 1, \ldots, l$ for the point observations. If residual systematic biases remain in the measurements, e.g., due to imperfect camera calibration, or model inaccuracies, then Equation (85) is not valid. According to Equations (76) and (77), such biases propagate approximately linearly through the error model, yielding a persistent offset in the rotation and translation estimates. These effects can be mitigated by improved calibration procedures to explicitly compensate for bias. When measurements are extracted from the same image frame, they may share common error sources such as global illumination variations, motion blur, or feature extraction uncertainties. This may violate Equation (90). Consequently, additional cross-correlation terms appear in the covariance derivation. In this case, our analytical formula would underestimate the true covariance, yielding overly confident uncertainty bounds. The magnitude of underestimation depends on both the correlation coefficient and the observation geometry. Additionally, in most practical scenarios, body and reference observations originate from distinct sources, onboard sensors, and prior models, and can be reasonably assumed independent. However, if both are derived from closely related image sources, e.g., sequential images processed with different algorithms, Equation (91) may be violated, introducing additional off-diagonal covariance terms that marginally increase total estimation uncertainty. Therefore, for real vision-based systems, we recommend characterizing actual error statistics through sensor testing to quantify biases and correlations. If treating our analytical covariances as lower bounds when positive correlations are suspected.

3.3.2. Derivation of the Moments

Applying the expectation operator on both sides of (76) and recalling that all true quantities are deterministic yields:

$$\begin{aligned} E\{\boldsymbol{\delta\theta}\} &= 2\left[\frac{1}{2}\lambda_0 I_3 - (B_{0n} + B_{0p} - 2B_0)\right]^{-1} E\{\Delta Z + \Delta Z_n + \Delta Z_p\} \\ &= 2\left[\frac{1}{2}\lambda_0 I_3 - (B_{0n} + B_{0p} - 2B_0)\right]^{-1} \left(E\{\Delta Z\} + E\{\Delta Z_n\} + E\{\Delta Z_p\}\right) \\ &= \mathbf{0_3} \end{aligned} \tag{92}$$

The expectations of the variables in the RHS of (92) are zero because, as seen from (82)–(84), the variables ΔZ, ΔZ_n, and ΔZ_p are deterministic linear mappings of unbiased random errors. Consider the translation estimation error, $\mathbf{\Delta t}$, in (77). Taking the expectation on both sides of the equation yields

$$\begin{aligned} E\{\mathbf{\Delta t}\} &= \frac{2}{\beta}\left[\left(\sum_{i=1}^{l} \beta_i [\mathrm{p}_{\mathrm{b_i}}^t \times]\right) E\{\boldsymbol{\delta\theta}\} - E\{\sum_{i=1}^{l} \beta_i (\Delta \mathrm{p}_{\mathrm{r_i}} - \Delta \mathrm{p}_{\mathrm{b_i}})\}\right] \\ &= \mathbf{0_3} \end{aligned} \tag{93}$$

where the first line stems from the deterministic nature of the true point observations, and the second line from the unbiasedness of the point observation errors and of the rotation estimation error.

Let $P_{\delta\boldsymbol{\theta}}$ denote the covariance matrix of the estimation error $\delta\theta$. Since it is unbiased, the following identity holds:

$$P_{\delta\boldsymbol{\theta}} = E\{\boldsymbol{\delta\theta}\boldsymbol{\delta\theta}^T\} \tag{94}$$

Rewriting for simplicity, the expression for $\delta\theta$ is as follows:

$$\boldsymbol{\delta\theta} = B_\theta(\Delta Z + \Delta Z_n + \Delta Z_p) \tag{95}$$

where

$$B_\theta = 2[\frac{1}{2}\lambda_0 I_3 - (B_{0n} + B_{0p} - 2B_0)]^{-1} \tag{96}$$

yields the following expression for $P_{\delta\boldsymbol{\theta}}$:

$$P_{\delta\boldsymbol{\theta}} = B_\theta \operatorname{cov}\{\Delta Z + \Delta Z_n + \Delta Z_p\} B_\theta^T \tag{97}$$

The derivation of the covariance matrix of the error terms $\Delta Z + \Delta Z_n + \Delta Z_p$ is lengthy but straightforward and is omitted here for the sake of brevity. Using (86)–(91), it can be shown that $P_{\delta\boldsymbol{\theta}}$ lends itself to the following expression:

$$\begin{aligned} P_{\delta\boldsymbol{\theta}} = B_\theta \Bigg(& \sum_{i=1}^{k} {\alpha_i}^2 [\mathrm{n}_{\mathrm{b}_i}^t \times](R_{\mathrm{n}_{\mathrm{b}_i}} + R_{\mathrm{n}_{\mathrm{r}_i}})[\mathrm{n}_{\mathrm{b}_i}^t \times]^T \\ & + \sum_{i=1}^{l} {\beta_i}^2 [\mathrm{p}_{\mathrm{b}_i}^t \times](R_{\mathrm{p}_{\mathrm{b}_i}} + R_{\mathrm{p}_{\mathrm{r}_i}})[\mathrm{p}_{\mathrm{b}_i}^t \times]^T \\ & + \frac{2}{\beta} \sum_{i,j=1}^{l} {\beta_i}^2 \beta_j [\mathrm{p}_{\mathrm{b}_i}^t \times](R_{\mathrm{p}_{\mathrm{b}_i}} + R_{\mathrm{p}_{\mathrm{r}_i}})[\mathrm{p}_{\mathrm{b}_j}^t \times]^T \\ & + \frac{1}{\beta^2} \sum_{i,j,m=1}^{l} {\beta_i}^2 {\beta_j}^2 [\mathrm{p}_{\mathrm{b}_i}^t \times](R_{\mathrm{p}_{\mathrm{b}_i}} + R_{\mathrm{p}_{\mathrm{r}_i}})[\mathrm{p}_{\mathrm{b}_m}^t \times]^T \Bigg) B_\theta^T \end{aligned} \tag{98}$$

Let $P_{\mathbf{\Delta t}}$ denote the covariance matrix of the translation error; then the following identity holds due to the unbiasedness property:

$$P_{\mathbf{\Delta t}} = E\{\mathbf{\Delta t}\mathbf{\Delta t}^T\} \tag{99}$$

Using (77) in (99) and exploiting the correlation assumptions in (86)–(91) yields the following expression for $P_{\mathbf{\Delta t}}$:

$$\begin{aligned} P_{\mathbf{\Delta t}} = \frac{4}{\beta^2} \Bigg[& \sum_{i=1}^{l} {\beta_i}^2 [\mathrm{p}_{\mathrm{b}_i}^t \times]\, P_{\delta\boldsymbol{\theta}} [\mathrm{p}_{\mathrm{b}_i}^t \times]^T + \sum_{i=1}^{l} {\beta_i}^2 (R_{\mathrm{p}_{\mathrm{b}_i}} + R_{\mathrm{p}_{\mathrm{r}_i}}) \\ & + \left(\sum_{i=1}^{l} \beta_i [\mathrm{p}_{\mathrm{b}_i}^t \times] \right) B_\theta \left(\sum_{j=1}^{l} {\beta_j}^2 [\mathrm{p}_{\mathrm{b}_j}^t \times](R_{\mathrm{p}_{\mathrm{r}_j}} + R_{\mathrm{p}_{\mathrm{b}_j}}) \right) \\ & + \left(\sum_{i=1}^{l} \beta_i [\mathrm{p}_{\mathrm{b}_i}^t \times] \right) B_\theta \left(\sum_{j=1}^{l} {\beta_j}^2 [\mathrm{p}_{\mathrm{b}_j}^t \times](R_{\mathrm{p}_{\mathrm{r}_j}} + R_{\mathrm{p}_{\mathrm{b}_j}}) \right)^T \\ & + \left(\sum_{i=1}^{l} \beta_i [\mathrm{p}_{\mathrm{b}_i}^t \times] \right) B_\theta \left(-\frac{1}{\beta} \sum_{i,j=1}^{l} \beta_i {\beta_j}^2 [\mathrm{p}_{\mathrm{b}_i}^t \times](R_{\mathrm{p}_{\mathrm{r}_j}} + R_{\mathrm{p}_{\mathrm{b}_j}}) \right) \\ & + \left(\sum_{i=1}^{l} \beta_i [\mathrm{p}_{\mathrm{b}_i}^t \times] \right) B_\theta \left(-\frac{1}{\beta} \sum_{i,j=1}^{l} \beta_i {\beta_j}^2 [\mathrm{p}_{\mathrm{b}_i}^t \times](R_{\mathrm{p}_{\mathrm{r}_j}} + R_{\mathrm{p}_{\mathrm{b}_j}}) \right)^T \\ & + \frac{2}{\beta} \sum_{i,j=1}^{l} {\beta_i}^2 \beta_j [\mathrm{p}_{\mathrm{b}_i}^t \times](R_{\mathrm{p}_{\mathrm{b}_i}} + R_{\mathrm{p}_{\mathrm{r}_i}})[\mathrm{p}_{\mathrm{b}_j}^t \times]^T \Bigg] \end{aligned} \tag{100}$$

3.4. Concluding Remarks

Equations (98) and (100) constitute the main results of this section. Expressions for the covariance matrices of the estimation errors of the dual quaternion estimator, which are provided here for the first time, constitute a necessary tool alongside the algorithm itself. Thanks to these matrices, practitioners may assess the expected accuracy of the pose

estimates, which is arguably as important as the estimates themselves. The covariance matrices may also be used to design appropriate sets of coefficients in weighing the relative importance of the point and vector observations. A particular case is presented here, where body and reference vector observation noise have identical covariance matrices, body and reference point observations have identical covariances, and these matrices are scaled identity matrices. These assumptions are expressed as follows:

$$R_{\mathrm{n_{b_i}}} = R_{\mathrm{n_{r_i}}} = \sigma_{\mathrm{n}}^2 I_3 \tag{101}$$

$$R_{\mathrm{p_{b_i}}} = R_{\mathrm{p_{b_i}}} = \sigma_{\mathrm{p}}^2 I_3 \tag{102}$$

These assumptions can be justified in some cases, e.g., in vision-based observations. Using (101) and (102) in (98) and (100) yields simplified expressions for $P_{\delta\boldsymbol{\theta}}$ and $P_{\mathbf{\Delta t}}$, respectively:

$$P_{\delta\boldsymbol{\theta}} = B_\theta \left(2\sigma_{\mathrm{n}}^2 \sum_{i=1}^{k} {\alpha_i}^2 [\mathrm{n}_{\mathrm{b_i}}^t \times][\mathrm{n}_{\mathrm{b_i}}^t \times]^T + 2\sigma_{\mathrm{p}}^2 \sum_{i=1}^{l} {\beta_i}^2 [\mathrm{p}_{\mathrm{b_i}}^t \times][\mathrm{p}_{\mathrm{b_i}}^t \times]^T + \frac{4\sigma_{\mathrm{p}}^2}{\beta} \sum_{i,j=1}^{l} {\beta_i}^2 \beta_j [\mathrm{p}_{\mathrm{b_i}}^t \times][\mathrm{p}_{\mathrm{b_j}}^t \times]^T + \frac{2\sigma_{\mathrm{p}}^2}{\beta^2} \sum_{i,j,m=1}^{l} {\beta_i}^2 {\beta_j}^2 [\mathrm{p}_{\mathrm{b_i}}^t \times][\mathrm{p}_{\mathrm{b_m}}^t \times]^T \right) B_\theta^T \tag{103}$$

$$\begin{aligned} P_{\mathbf{\Delta t}} = \frac{4}{\beta^2} \Bigg[& \sum_{i=1}^{l} {\beta_i}^2 [\mathrm{p}_{\mathrm{b_i}}^t \times]\, P_{\delta\boldsymbol{\theta}} [\mathrm{p}_{\mathrm{b_i}}^t \times]^T + 2\sigma_{\mathrm{p}}^2 \sum_{i=1}^{l} {\beta_i}^2 I_3 + \frac{4\sigma_{\mathrm{p}}^2}{\beta} \sum_{i,j=1}^{l} {\beta_i}^2 \beta_j [\mathrm{p}_{\mathrm{b_i}}^t \times][\mathrm{p}_{\mathrm{b_j}}^t \times]^T \\ & + 2\sigma_{\mathrm{p}}^2 \left((\sum_{i=1}^{l} \beta_i [\mathrm{p}_{\mathrm{b_i}}^t \times])\, B_\theta (\sum_{j=1}^{l} {\beta_j}^2 [\mathrm{p}_{\mathrm{b_j}}^t \times]) \right) + 2\sigma_{\mathrm{p}}^2 \left((\sum_{i=1}^{l} \beta_i [\mathrm{p}_{\mathrm{b_i}}^t \times])\, B_\theta (\sum_{j=1}^{l} {\beta_j}^2 [\mathrm{p}_{\mathrm{b_j}}^t \times]) \right)^T \\ & - \frac{2\sigma_{\mathrm{p}}^2}{\beta} \left((\sum_{i=1}^{l} \beta_i [\mathrm{p}_{\mathrm{b_i}}^t \times])\, B_\theta (\sum_{i,j=1}^{l} \beta_i {\beta_j}^2 [\mathrm{p}_{\mathrm{b_i}}^t \times]) \right) - \frac{2\sigma_{\mathrm{p}}^2}{\beta} \left((\sum_{i=1}^{l} \beta_i [\mathrm{p}_{\mathrm{b_i}}^t \times])\, B_\theta (\sum_{i,j=1}^{l} \beta_i {\beta_j}^2 [\mathrm{p}_{\mathrm{b_i}}^t \times]) \right)^T \Bigg] \end{aligned} \tag{104}$$

Fundamental insights into the algorithm performances are provided by (103) and (104) thanks to the clear separation between the geometry effect and the noise effect. This can be exploited in an optimal design of the weighting coefficients α_i and β_i, such as to balance measurement reliability and geometric diversity.

The error analysis presented in this section relies on a small error assumption, which posits that the vector observation errors $\Delta\mathrm{n}_{\mathrm{r_i}}, \Delta\mathrm{n}_{\mathrm{b_i}}$ and point observation errors $\Delta\mathrm{p}_{\mathrm{r_i}}, \Delta\mathrm{p}_{\mathrm{b_i}}$ are of small magnitude compared with the magnitude of the nominal (true) observations. Hence, the assumption is really holding for small angular deviations between the observations are their true counterparts. This widely adopted assumption allows us to obtain closed-form solutions by linearizing the error equations and consequently neglecting second-order and higher-order terms. Extensive numerical testing showed that the nonlinear estimator can perform with angular deviations up to 10^{-1} radians, while higher values would, in general, yield unreliable results, although not necessarily cause divergence. In a typical spacecraft mid-grade vision-based navigation systems, the vector measurement noise exhibits standard deviations in the order of $\sigma_n \sim 10^{-2}$ radians (about 0.5 degrees), while point measurement noise satisfies $\sigma_p \sim 10^{-2}$ meters for observations at distances of order 1–10 m. A previous work [12] on error analysis of the attitude quaternion estimation from vector observations provides crucial validation for the first-order approximation approach. The study derived second-order formulas for the error and for its bias, along with the second-order and fourth-order expressions for the covariance matrix. The key finding was that, for the case of zero-mean errors with standard deviation σ_n radians, the resulting bias exhibits a magnitude of order σ_n^2, and the attitude error covariance matrix features

diagonal elements of order σ_n^2 rad^2. The dual quaternion estimator studied in this work exhibits similar scaling behavior. The covariance expressions in Equations (98) and (100) scale as $\mathcal{O}(\sigma^2)$ for measurement noise of order $\sigma \sim 10^{-2}$, while the neglected second-order contributions in both rotation and translation errors would introduce corrections of order $\mathcal{O}(\sigma^4) \sim 10^{-8}$. They are, thus, negligible for practical purposes, and the linear approximation remains adequate for the levels of measurement noise typical of most spacecraft sensors.

4. Simulation Results

This section aims, first, to verify the statistical consistency of the error analysis presented previously and to demonstrate the algorithm's performance on a particular application case that is typical in close-range relative satellite navigation. Assume two spacecraft flying in a close formation-flight scenario as illustrated in Figure 1. The chaser spacecraft must determine its relative pose with respect to the target spacecraft based on single-frame images acquired by its onboard camera. Each image is processed to extract batches of point and vector observations described in the camera body frame, i.e., the $\mathcal{B}$ frame, which is rigidly attached to the chaser body frame. Each body point/vector observation is associated with a corresponding point/vector observation described in the target coordinates frame, which has the role of reference coordinate frame $\mathcal{R}$. Vector observations are, for instance, obtained as salient linear features on the target body, straight edges of solar arrays, an antenna's boresight, etc. Point observations are, for instance, corners of solar panels, vertices on a docking ring, active emitting light diodes, passive corner retroreflectors, etc.

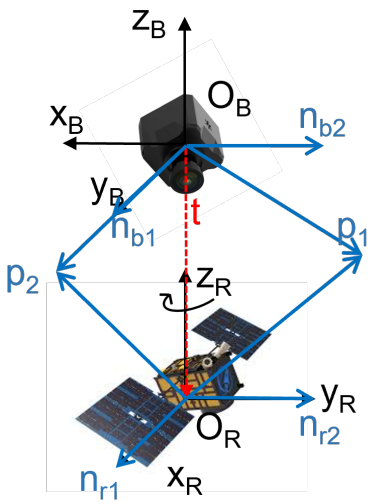


Figure 1. Scenario of a close-range formation flight. Single-frame images are processed onboard the chaser spacecraft. Two vector observations and two point observations are simultaneously processed to estimate the relative pose of the chaser spacecraft with respect to the target spacecraft.

First, using a particular geometry and batch of point and vector observations, Monte-Carlo simulations are performed through random generation of all possible noise terms to calculate empirical expectations of the nonlinear pose estimation errors and of the linearized errors. Similarly, the Monte-Carlo sample is used to evaluate the covariance matrices of the nonlinear pose errors and of the linearized errors. Comparison between these quantities, including the eigenvalues of the covariance matrices, yields the conclusion that the proposed error analysis indeed provides statistical consistency in the wide sense for the generic illustrative example. Further Monte-Carlo simulations are performed by randomly generating batches of point and vector observations, and the performances of the

proposed estimator are demonstrated by plotting the probability cumulative distribution function (CDF) of the pose estimation errors. Additional tests are performed to investigate the sensitivity of the pose estimation performance with respect to the number of vector and point observations. Comparison of the various configurations is made by plotting the various CDF. Finally, the rotation accuracy performance is benchmarked against that of the celebrated q-method applied to the same batch of vector observations.

4.1. Statistical Consistency

For verification of the statistical consistency of the error analysis, we choose a representative pose consisting of a rotation of -90 degrees about the target's z-axis and a translation vector coinciding with the $(-z)$-axis with a length of 2 m. It is as if the boresight of the chaser's camera were perfectly pointing to the target. A nearly minimal configuration of point and vector observations is selected, namely two vector observations and two point observations, see Figure 1. Let $(\mathrm{n}_{\mathrm{r}_1}, \mathrm{n}_{\mathrm{r}_2})$ and $(\mathrm{p}_{\mathrm{r}_1}, \mathrm{p}_{\mathrm{r}_2})$ denote the reference vector and point observations, respectively. The numerical values of these parameters are provided next.

$$
\begin{aligned}
\boldsymbol{q} &= \begin{bmatrix} 0 & 0 & -\frac{\sqrt{2}}{2} & \frac{\sqrt{2}}{2} \end{bmatrix} \\
\mathrm{t} &= \begin{bmatrix} 0 & 0 & -2 \end{bmatrix} [m] \\
\mathrm{n}_{\mathrm{r}_1} &= \begin{bmatrix} 1 & 0 & 0 \end{bmatrix} \\
\mathrm{n}_{\mathrm{r}_2} &= \begin{bmatrix} 0 & 1 & 0 \end{bmatrix} \\
\mathrm{p}_{\mathrm{r}_1} &= \begin{bmatrix} -2 & 2 & 0 \end{bmatrix} [m] \\
\mathrm{p}_{\mathrm{r}_2} &= \begin{bmatrix} 2 & 0 & 2 \end{bmatrix} [m]
\end{aligned}
$$

The true reference vector observations are corrupted by an additive zero-mean Gaussian noise, $\Delta\mathrm{n}_{\mathrm{r}_i}$. They are transformed to the body frame and corrupted with an additive zero-mean Gaussian noise, $\Delta\mathrm{n}_{\mathrm{b}_i}$. Both noises have the same equivalent angular standard deviation of $\sigma_{\mathrm{n}} = 0.01$ radians. This level is typical of mid-resolution imagers. Similarly, the true reference point observations are corrupted by an additive zero-mean Gaussian noise, $\Delta\mathrm{p}_{\mathrm{r}_i}$. They are transformed to the body frame and corrupted with an additive zero-mean Gaussian noise, $\Delta\mathrm{p}_{\mathrm{b}_i}$. Both errors have the same standard deviation of $\sigma_{\mathrm{p}} = 0.01$ m, reflecting typical uncertainties of mid-resolution camera-based systems. In this study, we assume that all covariance matrices are scaled identity matrices, i.e.,

$$
\begin{aligned}
R_{\mathrm{n}_{\mathrm{b}_i}} &= \sigma_{\mathrm{n}}^2 I_3 \\
R_{\mathrm{n}_{\mathrm{r}_i}} &= \sigma_{\mathrm{n}}^2 I_3 \\
R_{\mathrm{p}_{\mathrm{b}_i}} &= \sigma_{\mathrm{p}}^2 I_3 \\
R_{\mathrm{p}_{\mathrm{r}_i}} &= \sigma_{\mathrm{p}}^2 I_3
\end{aligned}
$$

Let $N = 100,000$ denote the number of Monte-Carlo runs in this study, i.e., the number of realizations of the quadruplet, $\Delta\mathrm{n}_{\mathrm{r}_i}$, $\Delta\mathrm{n}_{\mathrm{b}_i}$ $\Delta\mathrm{p}_{\mathrm{r}_i}$, $\Delta\mathrm{p}_{\mathrm{b}_i}$. The estimator applied here is the algorithm described in Section 2 with weighing coefficients $\alpha_i = \beta_i = 1$, for $i = 1, 2$. For each trial, the estimator calculates an estimate of the pose dual quaternion $\hat{q}_i$, extracts the

rotation quaternion, $\hat{\boldsymbol{q}}_i$, and the estimated translation $\hat{\mathbf{t}}_i$, and the nonlinear rotation and translation errors are calculated as follows:

$$\begin{bmatrix} \frac{1}{2}\delta\boldsymbol{\theta}_i^{NL} \\ 1 \end{bmatrix} = \boldsymbol{q}^{t^*} \odot \hat{\boldsymbol{q}}_i \tag{105}$$

$$\Delta\mathbf{t}_i^{NL} = \hat{\mathbf{t}}_\mathbf{i} - \mathbf{t} \tag{106}$$

$i = 1, 2, \ldots, N$. In parallel, the linear errors developed in (76) and (77) are evaluated at each trial:

$$\delta\boldsymbol{\theta}_j = B_\theta \left(\Delta Z_n + \Delta Z_p + \Delta Z\right)_j \tag{107}$$

$$\Delta\mathbf{t}_j = \frac{2}{\beta}\left[\sum_{i=1}^{l} \beta_i [\mathrm{p}_{\mathrm{b_i}}^t \times]\right] \delta\boldsymbol{\theta}_j - \sum_{i=1}^{l} \beta_i \left(\Delta \mathrm{p}_{\mathrm{r_i}} - \Delta \mathrm{p}_{\mathrm{b_i}}\right)_j \tag{108}$$

$j = 1, 2, \ldots, N$. Two measures of the biases are then calculated via the sample averages of the nonlinear and linear errors, i.e.,

$$\bar{\delta\boldsymbol{\theta}}^{MC} = \frac{1}{N}\sum_{i=1}^{N} \delta\boldsymbol{\theta}_i^{NL} \tag{109}$$

$$\bar{\delta\boldsymbol{\theta}} = \frac{1}{N}\sum_{j=1}^{N} \delta\boldsymbol{\theta}_j \tag{110}$$

and

$$\bar{\Delta\mathbf{t}}^{MC} = \frac{1}{N}\sum_{i=1}^{N} \Delta\mathbf{t}_i^{NL} \tag{111}$$

$$\bar{\Delta\mathbf{t}} = \frac{1}{N}\sum_{j=1}^{N} \Delta\mathbf{t}_j \tag{112}$$

Table 1 shows the value of the empirical biases in rotation and translation. It is seen from the first column that there are biases in the rotation estimates in all three axes, which is expected given the nonlinear nature of the estimator. These biases are, however, very small compared to the raw measurement noise standard deviation, which validates the unbiasedness result of the linear analysis. Indeed, the biases are of the order of 10^{-4} radian, which is an expected result as explained later. Moreover, the biases are very well predicted by the biases in the second column. It may appear at first surprising that the linear errors are biased, since the previous analysis showed them to be unbiased. This is explained as follows. The true values of the point and vector observations are not available and are thus replaced by their measured values. These noisy measured values are, in turn, multiplied by the noise. The vector noise has a standard deviation of 10^{-2} radian. The point noise has a standard deviation of 10^{-2} meters for lengths that are of the order of 1 m; this creates an equivalent angular standard deviation of 10^{-2} radian. The accumulation of vector and point observation errors, both of order 10^{-2} radian, along with the squaring effect of using noisy quantities, can explain the magnitude of 10^{-4} radian in the empirical biases. The excellent consistency between the empirical rotation biases in the first two columns of Table 1 clearly speaks in favor of the linear rotation error formula (76). The third column in Table 1 depicts the translation biases $\bar{\Delta\mathbf{t}}^{MC}$ of the nonlinear errors. They are nonzero since the estimator is indeed nonlinear; the estimate of the translation vector is a quadratic function of the rotation estimate, which itself is the product of a nonlinear processing. Notice that these biases are of the order 10^{-4} meter in three axes, and that this is precisely

predicted by the empirical biases of the linear approximation (second column). That is explained as follows. The linear error in the translation vector is affine in $\delta\boldsymbol{\theta}$. The constant is an additive zero-mean Gaussian term, and the coefficient is a function of a true body point observation. The sample average cancels the zero-mean Gaussian term contribution. The true body point observation is replaced by its noisy version, but the additive noise is only slightly correlated with the estimation error $\delta\boldsymbol{\theta}$. Since the true body point observation is of the order of 1 m, the translational biases remain of the same order as the rotational biases (but with length dimensions).

Table 1. Biases in the pose estimation error. $\delta\boldsymbol{\theta}\,[rad]$, $\boldsymbol{\Delta t}\,[m]$.

$\bar{\delta\boldsymbol{\theta}}^{MC}\,(\times\mathbf{10^{-4}})$	$\bar{\delta\boldsymbol{\theta}}\,(\times\mathbf{10^{-4}})$	$\bar{\boldsymbol{\Delta t}}^{MC}\,(\times\mathbf{10^{-4}})$	$\bar{\boldsymbol{\Delta t}}\,(\times\mathbf{10^{-4}})$
$\begin{bmatrix} 0.2589 \\ 0.1196 \\ 0.0405 \end{bmatrix}$	$\begin{bmatrix} 0.1698 \\ 0.0407 \\ 0.1577 \end{bmatrix}$	$\begin{bmatrix} 1.0896 \\ -0.6871 \\ -0.9411 \end{bmatrix}$	$\begin{bmatrix} -0.0757 \\ 0.5222 \\ -0.2240 \end{bmatrix}$

Table 2 presents the empirical covariance matrices of the rotation estimation error. The first column ${P_{\delta\boldsymbol{\theta}}}^{MC}$ represents the sample covariance matrix computed from the nonlinear estimation errors across all N Monte Carlo trials, ($N = 100,000$).

$$ {P_{\delta\boldsymbol{\theta}}}^{MC} = \frac{1}{N-1}\sum_{i=1}^{N}(\delta\boldsymbol{\theta}_i^{NL} - \bar{\delta\boldsymbol{\theta}}^{MC})(\delta\boldsymbol{\theta}_i^{NL} - \bar{\delta\boldsymbol{\theta}}^{MC})^T, \tag{113} $$

The notation $\delta\boldsymbol{\theta}_i^{NL}$ emphasizes that these errors are obtained from the nonlinear estimator described in Section 2.3. It is the rotation error vector at the i-th Monte Carlo trial, obtained from the dual quaternion nonlinear estimator. In practice, this vector is computed from the quaternion multiplicative error Equation (105), and $\bar{\delta\boldsymbol{\theta}}^{MC}$ is the sample mean of these error vectors, see Equation (109). The second column $P_{\delta\boldsymbol{\theta}}$ displays the approximated covariance matrix of the linear error, see Equation (98). This analytical expression is an approximation to first order in the measurement errors. The third column shows the eigenvalues of both matrices.

Table 2. Covariance of the attitude estimation error.

${P_{\delta\boldsymbol{\theta}}}^{MC}\,(\times\mathbf{10^{-4}})$	$P_{\delta\boldsymbol{\theta}}\,(\times\mathbf{10^{-4}})$	**Eigenvalue of** ${P_{\delta\boldsymbol{\theta}}}^{MC}, P_{\delta\boldsymbol{\theta}}\,(\times\mathbf{10^{-4}})$
$\begin{bmatrix} 1.3996 & -0.4515 & 0.3636 \\ -0.4515 & 0.7267 & -0.1831 \\ 0.3636 & -0.1831 & 0.5464 \end{bmatrix}$	$\begin{bmatrix} 6.5919 & -2.1880 & 1.5867 \\ -2.1880 & 2.9462 & -0.9752 \\ 1.5867 & -0.9752 & 1.8347 \end{bmatrix}$	$\begin{bmatrix} 0.4101, 8.1590 \\ 0.5001, 1.9798 \\ 1.7626, 1.2340 \end{bmatrix}$

It appears that the variances in the diagonal of ${P_{\delta\boldsymbol{\theta}}}^{MC}$ are of the order 10^{-4} rad^2. That is expected since the squared standard deviations, σ_{n}^2 and σ_{p}^2, are of order 10^{-4}, the vector observations are unitized, and the point observation lengths are of order 1 m. Hence, the matrix ${P_{\delta\boldsymbol{\theta}}}^{MC}$ scaled by 10^{-4} appears as an Attitude Dilution of Precision coefficient in all three axes. The x-axis seems to be the most affected with a coefficient of $\sim$1.4, followed by the y-axis with $\sim$0.7, and the z-axis with $\sim$0.5. It shows that the specific geometric configuration of the vector and point measurements is beneficial in the y and z-axes and detrimental in the x-axis. It appears that the cross-correlations are relatively high and the diagonal factors of dilution are close to unity. These effects are likely related to the small number of observations in the proposed near-minimal configuration. The second column depicts the covariance matrix of the linear rotation estimation error. It predicts the covariance matrix of the actual nonlinear error with very good consistency.

Indeed, both have the same order of magnitude, 10^{-4} rad^2, and the same relative order of the factors of dilution among the three axes: the z-axis is the least affected, then the y-axis, then the x-axis. Furthermore, the cross-correlation elements appear to have the same relative significance. A calculation of the ratios between corresponding diagonal elements yields approximately 4.7 for the x-axis, 4.1 for the y-axis, and 3.4 for the z-axis, suggesting that the linear approximations of the covariances are about four times larger than their Monte Carlo counterparts. This conservatism is a blessing in disguise for practical applications since optimistic approximations are in general riskier outcomes. In any case, practitioners should use the closed-form analytical formulas, i.e., Equation (98), to obtain computationally efficient predictions of uncertainty bounds as preliminary design tools, and further tune them using simulations. Using these covariance matrices in extended Kalman filters or other sensor fusion frameworks might provide some safety margins for mission-critical navigation decisions. At any rate, ${P_{\delta\boldsymbol{\theta}}}^{MC}$ is, in practice, not amenable to calculation while $P_{\delta\boldsymbol{\theta}}$ is. The third column in the table shows the eigenvalues of both covariance matrices; both are well-conditioned with similar condition numbers (about 5–6). Notice that these empirical covariance matrices were calculated without compensating for the biases calculated earlier. Hence, a better interpretation of these matrices is as second-order moments of the estimation errors. Yet the compensation would be of the order of the biases squared, i.e., 10^{-8} rad^2, which is negligible for all practical purposes.

Table 3 summarizes similar results for the translational error. The first two columns are the empirical covariance matrices of the nonlinear and the linear estimation errors, respectively, calculated using $N = 100,000$ trials. The third column depicts their eigenvalues.

Table 3. Covariance of the translation estimation error.

${\boldsymbol{P_{\Delta t}}}^{MC}(\times 10^{-4})$	$\boldsymbol{P_{\Delta t}}\ (\times 10^{-4})$	Eigenvalue of ${\boldsymbol{P_{\Delta t}}}^{MC}$, $\boldsymbol{P_{\Delta t}}\ (\times 10^{-4})$
$\begin{bmatrix} 5.2938 & 1.0488 & -1.0348 \\ 1.0488 & 5.2391 & -1.2055 \\ -1.0348 & -1.2055 & 5.2149 \end{bmatrix}$	$\begin{bmatrix} 7.2190 & 4.9524 & 3.5578 \\ 4.9524 & 8.9121 & 5.8243 \\ 3.5578 & 5.8243 & 7.8915 \end{bmatrix}$	$\begin{bmatrix} 4.0214, 2.2774 \\ 4.2836, 4.0016 \\ 7.4428, 17.7435 \end{bmatrix}$

The variances in the nonlinear errors are all very close to one another, $\sim 5.2 \times 10^{-4}$ m^2 in the three axes, showing that the matrix is well-conditioned with almost perfect anisotropy in the distribution of the deviations. This almost equality among the variances is consistently reflected in the linear covariance matrix, with factors of Position Dilution of Precision equal 7.2, 8.9, and 7.9, in x, y, and z, respectively. The order of magnitude of 10^{-4} m^2 is reminiscent of the significance of the rotation estimation error in the calculations, and of the fact that all raw errors, whether in vector or in point observations, are of the same order of magnitude. The translation errors exhibit less conservatism (factors 1.4–1.7) compared to rotation errors (factors 3.4–4.7). The translation error comprises two distinct components: a direct contribution from point measurement noise and the observation geometry, and an indirect contribution through coupling with the rotation error. The linear approximation $P_{\boldsymbol{\Delta t}}$ provides a bound on the true nonlinear covariance ${P_{\boldsymbol{\Delta t}}}^{MC}$ that is tighter than its rotational counterpart rotation. There is, however, more cross-correlation among the axes. This is reflected in the slightly worse condition number for the linear covariance matrix. The linearization is likely the root cause that creates correlation among the three dimensions. All in all, there is a very good consistency between the empirical covariance matrices, both in the translation and in the rotation errors.

4.2. Evaluation of Performance

In this part of the numerical study, we aim to evaluate the estimator's performance in accuracy under a wide range of poses and observation scenarios. A Monte-Carlo simulation

with 100,000 trials was performed, where each trial is associated with a particular pose, a particular geometry of point and vector observations, and a particular quadruplet of noises in the reference/body point/vector observations. The relative orientation was generated by drawing quaternion components from a zero-mean, unit-covariance Gaussian distribution and subsequently normalizing to guarantee quaternion unity. The translation vectors were generated from a uniform distribution with support [0–10] meters per axis, which is typical for close satellite formation flight, or a final approach phase of a rendezvous and docking maneuver.

For each pose, a set of k unit vectors was uniformly randomly generated in the target frame, and corrupted by zero-mean Gaussian noises with standard deviations of 1 degree per axis. The true target vector observations were transformed to the chase frame and corrupted by additive zero-mean Gaussian noises of the same standard deviation. A set of l true target point observations was also uniformly randomly generated and corrupted by zero-mean Gaussian noises with standard deviation 5×10^{-3} meters. The true target point observations were transformed into the chaser's body frame and corrupted with zero-mean Gaussian noises with the same standard deviations. In the present case, the true attitude quaternion and true translation vector are different in each trial. The angular error $\boldsymbol{\delta\theta}$ and the translation error $\mathbf{\Delta t}$ are defined as follows:

$$\boldsymbol{\delta\theta}_i = 2 \arccos\left(\hat{\boldsymbol{q}}_i^{\,T} \boldsymbol{q}_i\right) \tag{114}$$

$$\mathbf{\Delta t}_i = \|\mathbf{t_i} - \hat{\mathbf{t}}_\mathbf{i}\| \tag{115}$$

In each trial, there are two unit vectors and two point observations. The weights α_i and β_i are varied across three different ratio configurations, defined in Table 4.

Table 4. Weight ratios of unit vector and point for different ratio configurations.

Ratio Configuration	$\boldsymbol{\alpha_i/\beta_i}$
R_1	10,000
R_2	1000
R_3	100
R_4	10
R_5	1
R_6	0.1
R_7	0.01
R_8	0.001
R_9	0.0001

A classical design for the weights in least-squares costs is to choose them inversely proportional to the measurement variance, i.e., $\alpha_i \propto 1/\sigma_\mathrm{n}^2$ and $\beta_i \propto 1/\sigma_\mathrm{p}^2$. This weighting scheme ensures that more reliable measurements, those with lower variance, contribute more strongly to the estimate. This prescription is valid up to a common scaling factor, i.e., multiplying all weights by the same constant does not change the solution. The relative weight ratio α_i/β_i is, therefore, what fundamentally determines how unit vectors are balanced versus point measurements. Our analytical covariance expressions reveal a nuanced relationship involving measurement geometry, which is naturally connected to the Geometric Dilution of Precision (GDOP) concept. Equations (98) and (100) indeed include GDOP terms that modulate the pose uncertainty. For instance, the multiplication terms such as $[\mathrm{n}_{\mathrm{b_i}}^t \times]$ and $[\mathrm{p}_{\mathrm{b_i}}^t \times]$ act as geometric modulation factors that project measurement errors perpendicular to the observation direction. The matrix B_θ aggregates the geometric information present in the observations and amplifies the observation noise.

Figure 2 depicts the CDFs of the angular and translation errors. It reveals that the estimator in configuration R_1, where higher weights are allocated to unit vectors, tends to slightly outperform the traditional q-method, where only unit vectors are processed. This is in itself a sanity check of a sort. Yet, configuration R_1 yields the poorest performance among the configurations tested. This indicates that over-reliance on unit vectors discards valuable translational information. In contrast, configurations R_5 and R_9, where point measurements are equally or more heavily weighted, achieve superior performance; they fully leverage the richer information content of point observations. The near identical CDFs for R_5 and R_9 indicate a saturation effect: once point measurements are adequately weighted ($\alpha_i/\beta_i \leq 1$), further increases provide diminishing returns. Figure 3 further explains this phenomenon. These curves cluster tightly when the ratio α_i/β_i decreases, achieving the best performance when $\alpha_i/\beta_i < 100$. The GDOP interpretation is that the geometric information from the point observations has been fully exploited. These findings might help the practitioner select the weights via a principled design based on measurement noise characteristics and geometric configuration, rather than using ad-hoc empirical tuning. The analytical covariances offer a computationally efficient approach for weight optimization, eliminating the need for extensive Monte Carlo simulations at each design iteration.

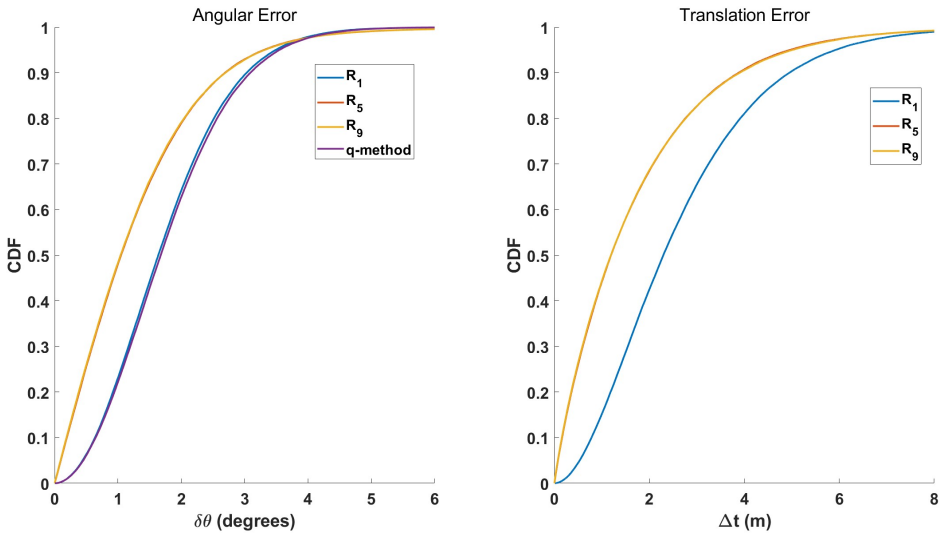


Figure 2. Pose error distributions under three weight configurations ($k = 2$, $l = 2$).

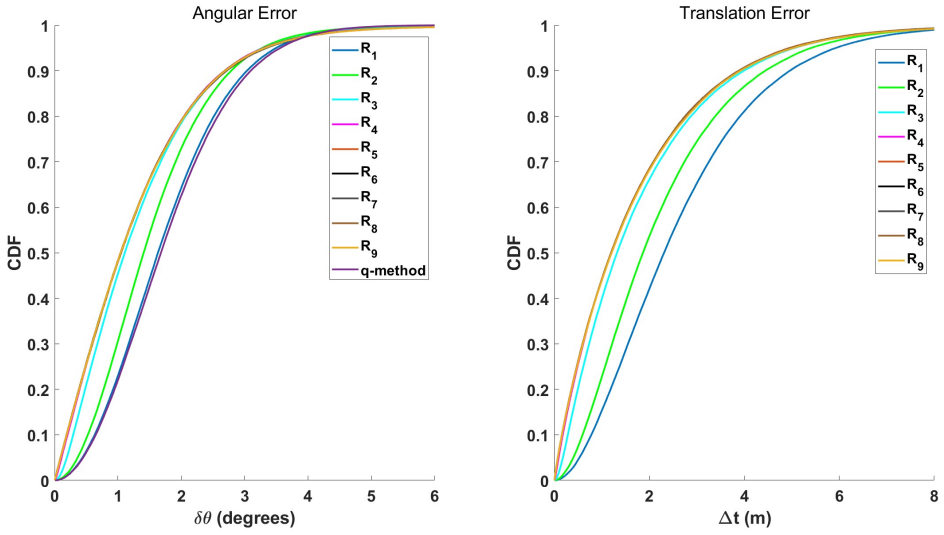


Figure 3. Pose error distributions for various weight configurations in the cost function ($k = 2$, $l = 2$).

Next, we study the impact of various dataset sizes. Figure 4 illustrates the impact of varying batch sizes on the estimator's performance. Increasing the number of measurements significantly improves the accuracy of both rotational and translational estimates. Notably, the CDF curve slowly improves once the number of point and vector observations exceeds 10. Although increasing input data enhances estimation accuracy, it also increases the computational load. A balance should be struck between computational speed and estimation accuracy, especially in scenarios where real-time processing is crucial.

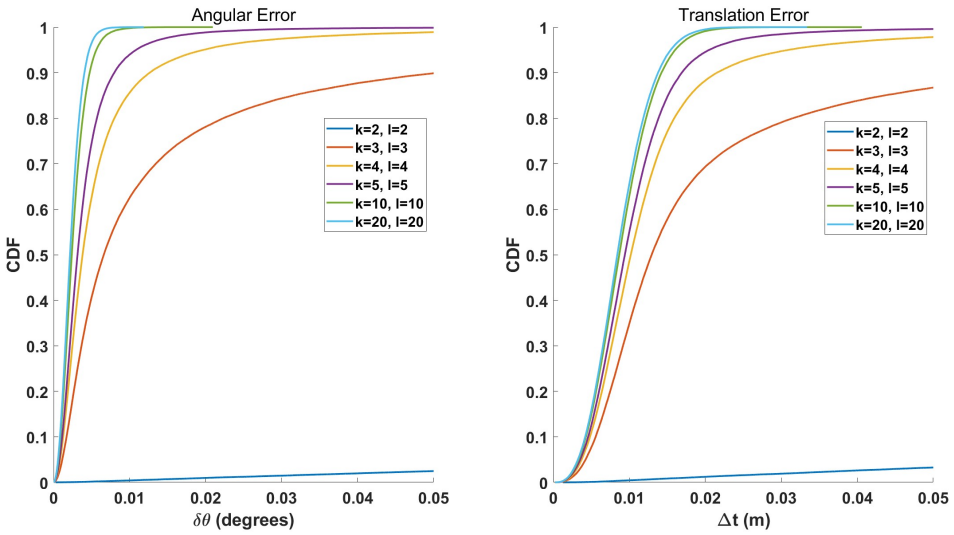


Figure 4. Pose error distributions for various batch sizes.

5. Conclusions

This study focused on a dual quaternion pose estimator that processes batches of point and unit vector observations. The study's core contribution is the derivation of analytical expressions for the six-dimensional pose error vectors and their associated covariance matrices. The derived expressions offer quantitative insight into the sensitivity of the estimation error to the measurement noise and to the geometry dilution of precision. The theoretical expressions were validated through extensive MC simulations across various scenarios. The estimator's performance was illustrated via the angular and translation error CDF. Larger batch sizes obviously improve accuracy, but the improvement curve flattens once the size reaches a threshold. This study also showcases the significance of fine-tuning the weights in the cost function to balance the rotational and translational accuracy. While we focused on a batch single-frame estimator, the insights gained herein may be used toward the development of a recursive time-varying algorithm that leverages the computational efficiency of dual quaternion for continuous on-board pose determination. The error analysis and covariance expressions presented in this study provide the necessary statistical foundation for sensor fusion taking place, for instance, in Kalman filters. Using the proposed results in dynamic scenarios will further enhance autonomy and reliability in future satellite GNC systems.

Author Contributions: Conceptualization, D.C.; methodology, D.C.; software, C.P.; validation, C.P.; formal analysis, C.P.; investigation, C.P.; resources, D.C.; data curation, C.P.; writing—original draft preparation, C.P.; writing—review and editing, D.C.; visualization, C.P.; supervision, D.C. All authors have read and agreed to the published version of the manuscript.

Funding: This research received no external funding.

Data Availability Statement: The data presented in this study are available on request from the corresponding author.

Conflicts of Interest: The authors declare no conflicts of interest.

Abbreviations

The following abbreviations are used in this manuscript:

GNC	guidance, navigation, and control
MC	Monte Carlo
RHS	Right-Hand Side
CDF	Cumulative Distribution Function
GDOP	Geometric Dilution of Precision
SEA	Small Error Assumption
SNR	Signal-to-Noise Ratio

References

1. Hamilton, W.R. On Quaternions; or on a New System of Imaginaries in Algebra. *Lond. Edinb. Dublin Philos. Mag. J. Sci.* **1844**, *25*, 489–495. [CrossRef]
2. Clifford, W.K. Preliminary Sketch of Biquaternions. *Proc. Lond. Math. Soc.* **1871**, *1*, 381–395. [CrossRef]
3. Filipe, N.; Tsiotras, P. Adaptive Position and Attitude-Tracking Controller for Satellite Proximity Operations Using Dual Quaternion. *J. Guid. Control Dyn.* **2015**, *38*, 566–577. [CrossRef]
4. Zivan, Y.; Choukroun, D. Dual Quaternion Kalman Filtering and Observability Analysis for Satellite Relative Navigation with Line-of-Sight Measurements. *IEEE Trans. Aerosp. Electron. Syst.* **2021**, *58*, 754–765. [CrossRef]
5. Dong, H.; Hu, Q.; Akella, M.R. Dual Quaternion-based Spacecraft Autonomous Rendezvous and Docking under Six-Degree-of-Freedom Motion Constraints. *J. Guid. Control Dyn.* **2018**, *41*, 1150–1162. [CrossRef]
6. Wang, J.; Liang, H.; Sun, Z.; Zhang, S.; Liu, M. Finite-Time Control for Spacecraft Formation with Dual-Number-Based Description. *J. Guid. Control Dyn.* **2012**, *35*, 950–962. [CrossRef]
7. Arun, K.S.; Huang, T.S.; Blostein, S.D. Least-Squares Fitting of Two 3-D Point Sets. *IEEE Trans. Pattern Anal. Mach. Intell.* **1987**, *5*, 698–700. [CrossRef]
8. Linnainmaa, S.; Harwood, D.; Davis, L.S. Pose Determination of a Three-Dimensional Object Using Triangle Pairs. *IEEE Trans. Pattern Anal. Mach. Intell.* **2002**, *10*, 634–647. [CrossRef]
9. Walker, M.W.; Shao, L.; Volz, R.A. Estimating 3-D Location Parameters using Dual Number Quaternions. *CVGIP Image Underst.* **1991**, *54*, 358–367. [CrossRef]
10. Sharma, S.; D'Amico, S. Neural Network-Based Pose Estimation for Noncooperative Spacecraft Rendezvous. *IEEE Trans. Aerosp. Electron. Syst.* **2020**, *56*, 4638–4658. [CrossRef]
11. Markley, F.L.; Crassidis, J.L. *Fundamentals of Spacecraft Attitude Determination and Control*; Springer: New York, NY, USA, 2014.
12. Choukroun, D.; Peng, C. Attitude Quaternion Estimation from Two Vector Observations. *J. Guid. Control Dyn.* **2025**, *48*, 700–706. [CrossRef]

Disclaimer/Publisher's Note: The statements, opinions and data contained in all publications are solely those of the individual author(s) and contributor(s) and not of MDPI and/or the editor(s). MDPI and/or the editor(s) disclaim responsibility for any injury to people or property resulting from any ideas, methods, instructions or products referred to in the content.